Experiments in Calibration of an Inertial Measurement Unit for UUV Applications

Daniel J. Stilwell* David J. Campbell

Systems Engineering Department
United States Naval Academy
Annapolis, MD 21402-5025
*stilwell@usna.edu

Abstract— *Gyro calibration techniques are investigated for a small, mid-grade inertial measurement unit suitable for UUV applications. Our goal is to characterize calibration requirements and techniques for small unmanned underwater vehicles that are deployed without reference to a master inertial system. As a first step toward this goal, we examine calibration techniques that use either Earth's rotation rate, or local pitch, roll, and heading sensors, as a reference.*

I. Introduction

Our goal is to rapidly and opportunistically deploy small unmanned underwater vehicles (UUVs). Toward this goal, we are investigating requirements for aligning and calibrating small, inexpensive guidance systems without the need for a master inertial reference system. This paper reports our first efforts to understand calibration of the gyros in a mid-grade inertial measurement unit.

Guidance system calibration for unmanned vehicles appears in both the UUV literature and the ground vehicle literature. In [4], on-line electronic compass calibration is addressed for a UUV, and in [10] on-line single-axis gyro calibration is addressed for a micro UUV. In [5] and [7], calibration of a mid-grade inertial measurement unit (IMU) is addressed for ground vehicle applications. In [11], several calibration tests are considered for a small IMU/GPS navigation package integrated via complementary filters.

In this work, we concentrate exclusively on gyro bias calibration for a mid-grade IMU. A least-squares technique is considered where gyro bias is estimated by minimizing the error from a set of collected data. This is an off-line approach, but can be performed during deployment after a sufficient amount of data has been collected. While this approach yields a minimizing bias error, approximations to the true gyro dynamics are required to derive a closed-form solution. Another approach utilizes a nonlinear observer that asymptotically estimates the bias error in real-time. The observer accounts for the nonlinear gyro dynamics and no approximations are required.

II. Inertial measurement unit characterization

Initial experiments are designed to establish two parameters: time after start-up until the IMU reaches steady-state operation, and the amount of data that must be collected in order to ensure that the mean of the data has minimum noise.

Several hours of data are recorded while the instrument is at rest. A plot of the y-axis gyro output is shown in Figure 1. The points on the plots represent the mean of 5 minutes of data (the IMU produces 400 measurements per second). A moving average filter removes higher frequency noise so that low frequency trends are more clearly displayed. From Figure 1, the output of the y-axis gyro is essentially stationary after about 10 minutes. Though not shown here, we experimentally determined a similar trend for the remaining three gyro channels. From the results of this experiment, we impose a 10 minute warm-up period for the IMU in all subsequent experiments. The data shown in Figure 1 was collected when the IMU was in a sealed vessel, but not submerged. We anticipate a lower steady state temperature and smaller warm-up time when the IMU is submerged.

In a second static test, the mean of measurements is computed for a data collected over a fixed interval. This processes is repeated continuously, generating a sequence of means. We expect the sample standard deviation of the means to decrease by $1/\sqrt{T}$, where T is the time span corresponding to each set of measurements. For a sufficiently large interval T_o, the sample standard deviations of the means stop decreasing. During a bench-top test where a single number is needed to represent the output of an IMU channel, T_o is the length of time over which data should be collected and a mean computed. Figure 2 shows the standard deviation of the mean versus time interval for the y-axis gyro. The standard deviation of the mean stops decreasing when intervals are longer than 10 minutes. Thus for a static test, the mean should be computed from 10 minutes of measurements.

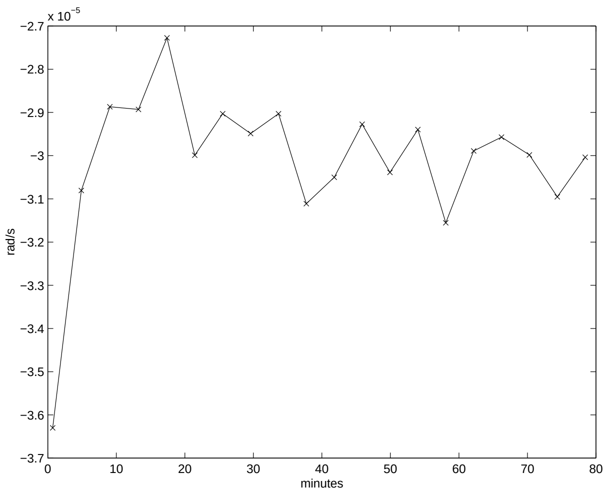

Fig. 1. Measured y-axis angular rate over time. Each point represents the mean of 5 minutes of data.

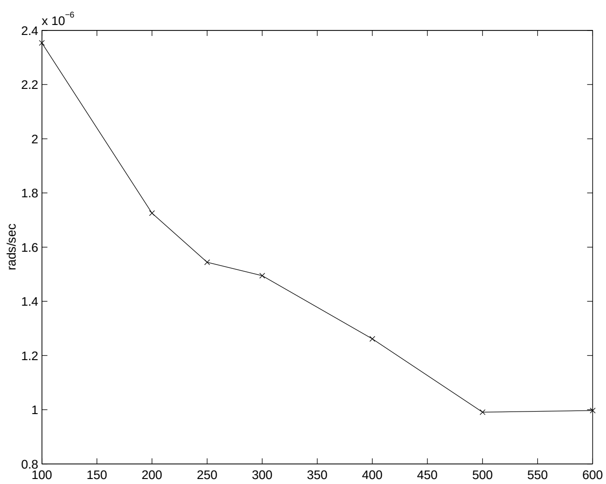

Fig. 2. Standard deviation of mean gyro output versus length of time over which each mean is computed.

III. Notation

The remainder of this paper addresses calibration three orthogonal gyros on an IMU, and we begin by briefly describing our notation and conventions. Angular rate of the IMU is denoted

$$\omega = \begin{bmatrix} \omega_x \\ \omega_y \\ \omega_z \end{bmatrix}$$

and is referred to as the body angular rate. Angular displacement of the IMU with respect to a local level (north-east-down) coordinate frame is described using Euler angles roll, pitch, and yaw, which we denote by ϕ, θ, and ψ, respectively. The vector of Euler angles is written $\eta = [\phi, \theta, \psi]^T$.

The rotation matrix $R \triangleq R(\eta) \in SO(3)$ that transforms vectors in the IMU coordinate frame to vectors in the local level frame satisfies $RR^T = I$, $\det(R) = 1$ and is written

$$R(\phi, \theta, \psi) \triangleq \begin{bmatrix} R_{1,1} & R_{1,2} & R_{1,3} \\ R_{2,1} & R_{2,2} & R_{2,3} \\ R_{3,1} & R_{3,2} & R_{3,3} \end{bmatrix} \tag{1}$$

where

$$\begin{aligned} R_{1,1} &= \cos(\theta)\cos(\psi) \\ R_{1,2} &= \sin(\phi)\sin(\theta)\cos(\psi) - \cos(\phi)\sin(\psi) \\ R_{1,3} &= \cos(\phi)\sin(\theta)\cos(\psi) + \sin(\phi)\sin(\psi) \\ R_{2,1} &= \cos(\theta)\sin(\psi) \\ R_{2,2} &= \sin(\phi)\sin(\theta)\sin(\psi) + \cos(\phi)\cos(\psi) \\ R_{2,3} &= \cos(\phi)\sin(\theta)\sin(\psi) - \sin(\phi)\cos(\psi) \\ R_{3,1} &= -\sin(\theta) \\ R_{3,2} &= \sin(\phi)\cos(\theta) \\ R_{3,3} &= \cos(\phi)\cos(\theta) \end{aligned}$$

IV. Angular rate and Euler parameters

We use three different representations for the differential relationship between body angular rate and Euler angles.

A. Euler angle integration

Euler angles are integrated directly using the relationship

$$\dot{\eta}(t) = Q(\eta(t))\omega(t) \tag{2}$$

where

$$Q(\eta) = \begin{bmatrix} 1 & \sin(\phi)\tan(\theta) & \cos(\phi)\tan(\theta) \\ 0 & \cos(\phi) & -\sin(\phi) \\ 0 & \sin(\phi)/\cos(\theta) & \cos(\phi)/\cos(\theta) \end{bmatrix}$$

The right-hand side of (2) has singularities at $\theta = 2(n-1)\pi$ for n an integer. Thus direct integration of Euler angles can be problematic in practice. We find (2) useful since the Euler parameters are generated directly as a result of integration, and a least squares approach to gyro bias estimation can be obtained.

B. Rotation matrix integration

A second representation of the differential relationship involves rotation matrices. The time-derivative of (1) satisfies

$$\dot{R}(t) = R(t)S(\omega(t)) \tag{3}$$

where

$$S(\omega) = \begin{bmatrix} 0 & -\omega_z & \omega_y \\ \omega_z & 0 & -\omega_x \\ -\omega_y & \omega_x & 0 \end{bmatrix} \tag{4}$$

is a skew-symmetric matrix representation of the cross product $(\omega\times)$. Euler angles are recovered from (1) using the relationships

$$\begin{aligned} \tan(\phi) &= \frac{R_{3,2}}{R_{3,3}} \\ \sin(\theta) &= -R_{3,1} \\ \tan(\psi) &= \frac{R_{2,1}}{R_{1,1}} \end{aligned}$$

C. Quaternion integration

The third approach uses unit quaternions, a four-element representation for the transformation matrices $SO(3)$ (the unit quaternion group is onto $SO(3)$, but not $1-1$). We partition a unit quaternion

$$q = \begin{bmatrix} v_o \\ v \end{bmatrix}$$

where $v_o \in \mathbb{R}$ and $v \in \mathbb{R}^3$. A unit quaternion q satisfies $\|q\| = \sqrt{v_o^2 + v^T v} = 1$. Let

$$x = \begin{bmatrix} v_{xo} \\ v_x \end{bmatrix}, \quad \text{and} \quad y = \begin{bmatrix} v_{yo} \\ v_y \end{bmatrix}$$

be unit quaternions, then the quaternion product is defined

$$x \cdot y = \begin{bmatrix} v_{xo} & -v_x^T \\ v_x & S(v_x) + Iv_{xo} \end{bmatrix} \begin{bmatrix} v_{yo} \\ v_y \end{bmatrix}$$

Note unit quaternions do not commute over the product operator. The identity unit quaternion is

$$q = \begin{bmatrix} 1 \\ 0 \\ 0 \\ 0 \end{bmatrix}$$

and the inverse of a unit quaternion is

$$q^{-1} = \begin{bmatrix} v_o \\ -v \end{bmatrix}$$

Integration of rotation matrices defined in (3) is expressed using unit quaternions as

$$\dot{q}(t) = \tfrac{1}{2} T(q(t))\omega(t) \tag{5}$$

where

$$T(q) = \begin{bmatrix} -v^T \\ S(v) + Iv_o \end{bmatrix}$$

and $q(t)$ is the unit quaternion corresponding to $R(t)$ in (3). Unit quaternions are transformed to rotation matrices using the relationships

$$\begin{aligned} R_{1,1} &= v_o^2 + v_1^2 - v_2^2 - v_3^2 \\ R_{1,2} &= 2(v_1 v_2 - v_o v_3) \\ R_{1,3} &= 2(v_1 v_3 + v_o v_2) \\ R_{2,1} &= 2(v_1 v_2 + v_o v_3) \\ R_{2,2} &= v_o^2 - v_1^2 + v_2^2 - v_3^2 \\ R_{2,3} &= 2(v_2 v_3 - v_o v_1) \\ R_{3,1} &= 2(v_1 v_3 - v_o v_2) \\ R_{3,2} &= 2(v_2 v_3 + v_o v_1) \\ R_{3,3} &= v_o^2 - v_1^2 - v_2^2 + v_3^2 \end{aligned}$$

Two properties of rotation matrices and quaternions are needed in the sequel,

Proposition IV.1: Let rotation matrices R_1 and R_2 satisfy

$$\dot{R}_1(t) = R_1(t)S(w_1(t))$$

and

$$\dot{R}_2(t) = R_2(t)S(w_2(t))$$

If $R_3 = R_2^T R_1$, then R_3 satisfies

$$\dot{R}_3(t) = R_3(t)S(w_1(t) - R_3^T w_2(t))$$

Proposition IV.2: Let $[v_o(t),\ v^T(t)]^T$ be a unit quaternion, then

$$v_o(t)\dot{v}_o(t) + v^T(t)\dot{v}(t) = 0$$

Advantages of integration via rotation matrices or unit quaternions is matter of debate [8]. For the purposes of our analysis, rotation matrix integration (3) has the desirable property of being described by a linear time-varying system. On the other hand, unit quaternion integration (5) has the property that angular rate enters the dynamics linearly.

V. Calibration

Let ω_I be the body angular rate measured by the IMU. We assume that the true body angular rate is

$$\omega(t) = \omega_I(t) + b + R^T(\eta)\omega_e$$

where $b \in \mathbb{R}^3$ is a *bias* error,

$$\omega_e = 7.2921 \times 10^{-5} \begin{bmatrix} \cos(L) \\ 0 \\ -\sin(L) \end{bmatrix}$$

is earth rate in the local level frame, and L is the local latitude.

The remainder of this paper concerns determination of the bias error b. We present three different methods for computing the bias error. Other error sources are possible and likely. These include scale factor errors, temperature dependence, non-orthogonality, and g-induced biases [1], [8].

A. Static bias estimate

If the exact orientation of the IMU is known, it is possible to calibrate the bias error by comparing the output of the gyro to earth-rate. A modification of this approach is suitable when north is difficult to determine.

If the IMU is level, the outputs of the two horizontal gyros are

$$\omega_{x_1} = 7.2921 \times 10^{-5} \cos(\psi)\cos(L) + b_x \qquad (6)$$

$$\omega_{y_1} = 7.2921 \times 10^{-5} \cos(\psi)\cos(L) + b_y \qquad (7)$$

If the IMU is rotated about the vertical axis by 180 degrees, then (6) and (7) yield

$$\omega_{x_2} = 7.2921 \times 10^{-5} \cos(\psi + \pi)\cos(L) + b_x \qquad (8)$$

$$\omega_{y_2} = 7.2921 \times 10^{-5} \cos(\psi + \pi)\cos(L) + b_y \qquad (9)$$

Summing (6) with (8) and (7) with (9) yields

$$b_x = \frac{\omega_{x_1} + \omega_{x_2}}{2}$$

$$b_y = \frac{\omega_{y_1} + \omega_{y_2}}{2}$$

Using this test, we computed

$$b_x = 4.3 \times 10^{-6}$$

$$b_y = -3.4 \times 10^{-7}$$

Bias for the remaining gyro is computing by repeating this test with the IMU rotated to place the remaining gyro axis in the horizontal plane.

VI. Dynamic calibration

When direct Euler angle measurements are available, the bias calibration can be computed from dynamic measurements.

A. Least squares

Let $\eta(k)$, $k = 1, \ldots, n$, be a set of discrete Euler angle measurements, and let $\hat{\eta}(k)$ be a corresponding set of Euler angle estimates obtained by integration of body angular rates using (2). A least squares estimate of the bias error $\hat{b}$ minimizes the functional

$$\sum_{i=0}^{n} \|\eta(i) - \hat{\eta}(i)\|^2$$

for a given estimate of the initial condition $\hat{\eta}(0)$. Although direct Euler angle integration is not typically implemented due to singularities, we choose Euler angle integration for the least squares problem since it directly relates the bias error in the body angular rate to Euler angles, which are the physical variables of interest.

Euler angle integration (2) is approximated in discrete-time as

$$\hat{\eta}(k+1) = \hat{\eta}(k) + hQ(\hat{\eta}(k))(\omega_I + b + R^T(\hat{\eta}(k))\omega_e)$$

where h is the sample period. Let $Q(k) \triangleq Q(\eta(k))$ and $R(k) \triangleq R(\eta(k))$, then for any subsequent time step,

$$\begin{aligned} \hat{\eta}(k+n) \approx \hat{\eta}(k) &+ h\sum_{i=k}^{n-1} Q(i)\left(\omega_I(i) + R^T(i)\omega_e\right) \\ &+ h\sum_{i=k}^{n-1} Q(i)b \end{aligned} \qquad (10)$$

The approximation in (10) arises from neglecting that b enters into $Q(\cdot)$ and $R(\cdot)$ through previous values of $\hat{\eta}(k)$. Note that we use $Q(\eta(k))$ and $R(\eta(k))$ instead of $Q(\hat{\eta}(k))$ and $R(\hat{\eta}(k))$. We find experimentally that this approximation results in reasonable estimates of b.

From (10), we construct the overdetermined system

$$y = Ab \qquad (11)$$

where

$$y = \begin{bmatrix} \eta(k+1) - \hat{\eta}(k) - hQ(k)\left(\omega_I(k) + R^T(k)\omega_e\right) \\ \vdots \\ \eta(k+n) - \hat{\eta}(k) - h\sum_{i=1}^{n-1} Q((i))\left(\omega_I(i) + R^T(i)\omega_e\right) \end{bmatrix} \qquad (12)$$

and

$$A = \begin{bmatrix} hQ(k) \\ \vdots \\ h\sum_{i=k}^{n-1} Q(i) \end{bmatrix}$$

From (12), the least squares estimate of b is

$$\hat{b} = (A^T A)^{-1} A^T y \tag{13}$$

B. Quaternion observer

A nonlinear observer can asymptotically estimate bias error without an approximation of the nonlinear gyro dynamics. Our observer is based on the attitude observer presented in [6]. An similar observer appears in [9] and was tested in simulation only. Our result differs largely with respect to the proof, and we verify the result with experimental data.

Let $\hat{R}$ be an estimate of the true rotation matrix R, and define the estimation error $\tilde{R} = \hat{R}^T R$. If the estimate is perfect, then $\tilde{R} = I$. Thus the observer must satisfy $\tilde{R}(t) \to I$ as $t \to \infty$. From (3), the observer is based on

$$\dot{R}(t) = R(t)S(\omega_I(t) + b + R^T(\eta(t))\omega_e) \tag{14}$$

Let $\hat{R}$ and $\hat{b}$ be estimates for R and b, respectively. Then an observer for (14) is

$$\begin{aligned} \dot{\hat{R}}(t) &= S(\tilde{R}(\omega_I(t) + \hat{b} \\ &\qquad + R^T(\eta(t))\omega_e + k_1 e(t)\,\mathrm{sgn}(e_o(t))) \qquad (15) \\ \dot{\hat{b}}(t) &= k_2 e(t)\,\mathrm{sgn}(e_o(t)) \qquad (16) \end{aligned}$$

where $[e_o,\ e^T]^T$ is the quaternion representation of the observer error $\tilde{R}$, and the signum function is defined $\mathrm{sgn}(e_o) = 1$ if $e_o \geq 0$ and $\mathrm{sgn}(e_o) = -1$ if $e_o < 0$.

Theorem VI.1: For any initial conditions $\hat{R}(0)$, $\hat{b}(0)$, and scalars $k_1 > 0$, $k_2 > 0$, $\|b(t) - \hat{b}(t)\| \to 0$ asymptotically.

Proof: Using property IV.1, the observer error $\tilde{R} = \hat{R}^T R$ satisfies

$$\begin{aligned} \dot{\tilde{R}}(t) &= \tilde{R}(t)S(\tilde{b} - k_1 e(t)\,\mathrm{sgn}(e_o(t))) \\ \dot{\tilde{b}}(t) &= -k_2 e(t)\,\mathrm{sgn}(e_o(t)) \end{aligned} \tag{17}$$

where $\tilde{b} = b - \hat{b}$ is bias estimation error. Using quaternions, (17) is equivalent to

$$\begin{aligned} \begin{bmatrix} \dot{e}_o(t) \\ \dot{e}(t) \end{bmatrix} &= \frac{1}{2}\begin{bmatrix} -e^T(t) \\ Ie_o(t) + S(e(t)) \end{bmatrix} \left(\tilde{b} - k_1 e(t)\,\mathrm{sgn}(e_o(t))\right) \\ \dot{\tilde{b}}(t) &= -k_2 e(t)\,\mathrm{sgn}(e_o(t)) \end{aligned} \tag{18}$$

To compute equilibria for (18), we note that $[e_o, e^T]^T$ is a unit quaternion and that $e_o^2 + e^T e = 1$. Thus (18) is written

$$\begin{aligned} \dot{e}_o(t) &= -\tfrac{1}{2}e^T(t)\tilde{b}(t) + \tfrac{1}{2}k_1(1 - e_0^2(t))\,\mathrm{sgn}(e_o(t)) \\ \dot{e}(t) &= \tfrac{1}{2}(e_o(t)I - S(e(t))(\tilde{b}(t) - k_1 e(t)\,\mathrm{sgn}(e_o(t))) \\ \dot{\tilde{b}}(t) &= -\tfrac{1}{2}k_2 e(t)\,\mathrm{sgn}(e_o(t)) \end{aligned} \tag{19}$$

From (19), the equilibria for the error dynamics are

$$\begin{bmatrix} e_o \\ e \\ \tilde{b} \end{bmatrix} = \begin{bmatrix} 1 \\ 0 \\ 0 \end{bmatrix}, \text{ or } \begin{bmatrix} e_o \\ e \\ \tilde{b} \end{bmatrix} = \begin{bmatrix} -1 \\ 0 \\ 0 \end{bmatrix}$$

both of which correspond to the same rotation matrix. To verify asymptotic stability, define $\nu = [e_o, e^T, \tilde{b}^T]^T$ and consider the Lyapunov function candidate

$$\begin{aligned} V(\nu(t)) &= \tilde{b}^T(t)\tilde{b}(t) \\ &\quad + \begin{cases} (e_o(t) - 1)^2 + e^T(t)e(t), & e_o(t) \geq 0 \\ (e_o(t) + 1)^2 + e^T(t)e(t), & e_o(t) \geq 0 \end{cases} \end{aligned}$$

Then using property IV.2

$$\begin{aligned} \dot{V}(\nu(t)) &= 2\tilde{b}^T(t)(-\tfrac{1}{2}k_2 e(t)\,\mathrm{sgn}(e_o(t))) \\ &\quad + \begin{cases} -2k_2\dot{e}_o(t), & e_o(t) \geq 0 \\ 2k_2\dot{e}_o(t), & e_o(t) \geq 0 \end{cases} \\ &= k_1 k_2 e^T(t)e(t) \end{aligned}$$

Thus $\dot{V}(\nu(t)) \leq 0$ for all $\nu(t)$. Define $\Omega = \{\nu | \dot{V}(\nu(t)) = 0\}$. For asymptotic stability, it remains to apply LaSalle's Theorem and show that $\nu(t)$ can only remain in Ω for all future time if $\nu(t)$ is at an equilibrium. Note that $\nu(t) \in \Omega$ if and only if $e(t) = 0$, thus $\nu(t) \in \Omega$ implies that

$$\begin{aligned} \dot{e}_o(t) &= \tfrac{1}{2}k_1(1 - e_o^2(t))\,\mathrm{sgn}(e_o(t)) \\ \dot{e}(t) &= \tfrac{1}{2}e_o(t)\tilde{b}(t) \\ \dot{\tilde{b}}(t) &= 0 \end{aligned}$$

If the error dynamics (18) are not at an equilibrium, then either $\dot{e}_o$ or $\dot{e}$ is nonzero. If $\dot{e}$ is nonzero, we are done. If $\dot{e}_o$ is nonzero, then $e_o^2 \neq 1$ and e cannot remain at zero since $e_o^2 + e^T e = 1$. Thus by LaSalle's Theorem, the error dynamics are asymptotically stable. ■

VII. Experiments

The bias estimation techniques presented in Section VI were experimentally tested using data collected during deployment of the Johns Hopkins University Remotely Operated Vehicle (JHUROV) at the United States Naval Academy Hydromechanics Laboratory. Euler angles were obtained from pitch and roll sensors, and from a gyro-stabilized magnetic compass on board the JHUROV. The IMU was deployed in an inertial guidance package mounted on the ROV. The inertial package was developed by USNA Midshipmen and is described in the Appendix.

Both bias estimation techniques are tested using Euler angle data that is shown in Figure 3 and corresponding body angular rates that are not shown. The vehicle remained in a fixed position and oscillated $\pm 5^o$ in yaw at $\frac{1}{8}$ Hz. After 340 seconds, the JHUROV increased yaw oscillation frequency to $\frac{1}{4}$ Hz. After 650 seconds, the vehicle ceased yaw oscillation and oscillated about $\frac{1}{2}$ meter in surge. By limiting the JHUROV to small motions, are intent was to limit errors in the compass measurements.

For both calibration techniques, the bias errors were computed from the first 340 seconds of data. Estimated Euler angles were then computed by integrating measured body angular rate over the entire data set using the estimated bias errors. Performance of the bias estimation techniques is evaluated by comparing the estimated Euler angles from those obtained by direct measurement.

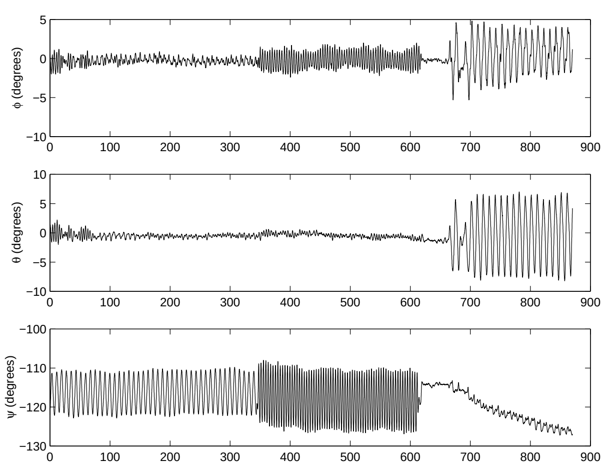

Fig. 3. True Euler angles as measured by the JHU ROV.

A. Least squares estimation

Least squares estimation (13) was applied to the first 340 seconds the data corresponding to Figure 3, yielding

$$\hat{b} = \begin{bmatrix} 7.7103 \times 10^{-5} \\ 5.4113 \times 10^{-6} \\ -3.0985 \times 10^{-5} \end{bmatrix} \tag{20}$$

The entire data set was integrated using the bias estimate (20). The absolute value of the error in each gyro is shown in Figure 4, along with the error when the bias estimate is zero. Improvement is seen in each axis except the y-axis . The least squares algorithm minimizes the root-sum-squared error of all three axes, not the error in individual axes. Let e_x, e_y, e_z be the error in each channel. The root-sum-squared error, $\sqrt{e_x^2 + e_y^2 + e_z^2}$, is shown in Figure 5.

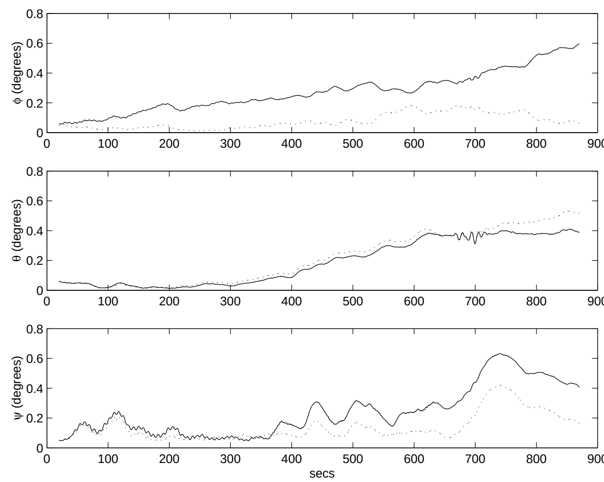

Fig. 4. Absolute value of Euler angle error with bias computed from least squares (- - - -), and zero bias (——). Data has been smoothed using a 10 second averaging window.

B. Observer

The observer (15) and (16) was implemented on the first 340 seconds of data corresponding to Figure 3, yielding

$$\hat{b} = \begin{bmatrix} 4.7527 \times 10^{-5} \\ 4.3960 \times 10^{-5} \\ -2.257 \times 10^{-5} \end{bmatrix} \tag{21}$$

The bias estimates are shown in Figure 6. After 340 seconds, the observer is stopped and the bias estimate is fixed at the current value. The entire data set was integrated again using the bias estimate (21). The absolute value of the error in each gyro is shown in Figure 7, along with the error when the bias estimate is zero. Improvement is seen in each axis except the y-axis . The root-sum-squared error, $\sqrt{e_x^2 + e_y^2 + e_z^2}$ is shown in Figure 8.

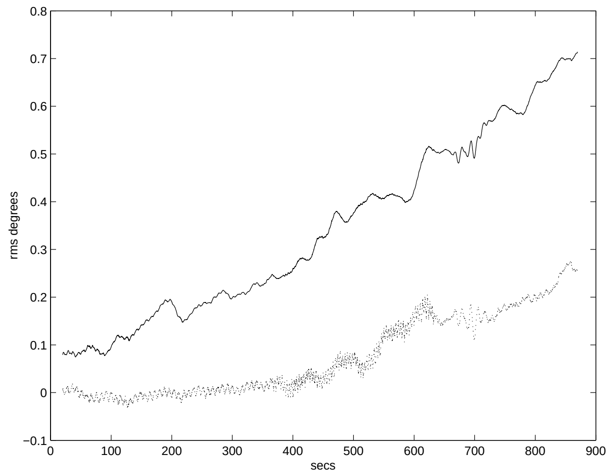

Fig. 5. Root sum square error with bias computed from least squares (- - - -), and zero bias (——). Data has been smoothed using a 10 second averaging window.

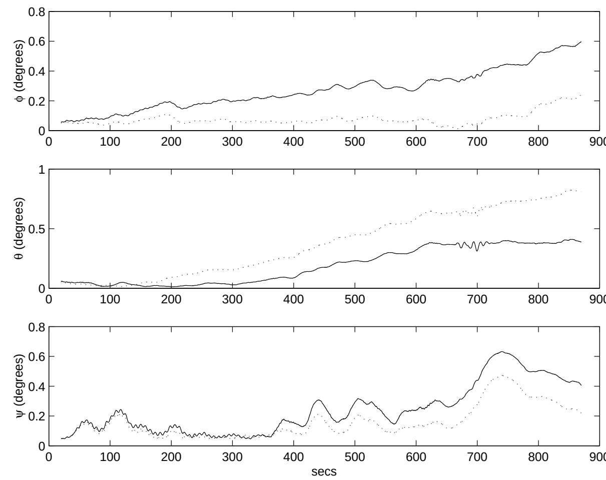

Fig. 7. Absolute value of Euler angle error with bias computed from nonlinear observer (- - - -), and zero bias (——). Data has been smoothed using a 10 second averaging window.

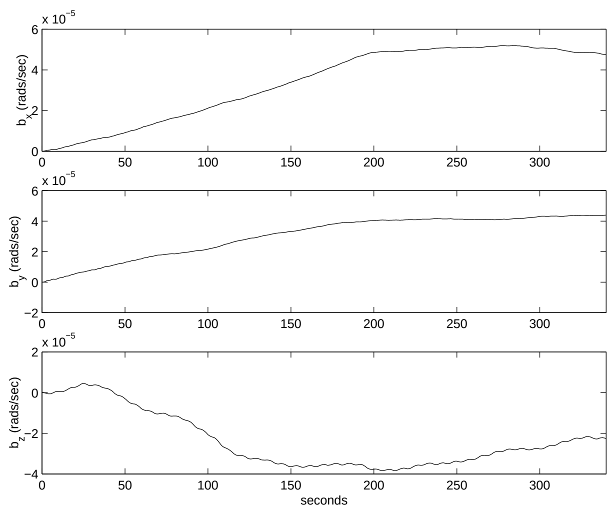

Fig. 6. Bias estimate from nonlinear observer.

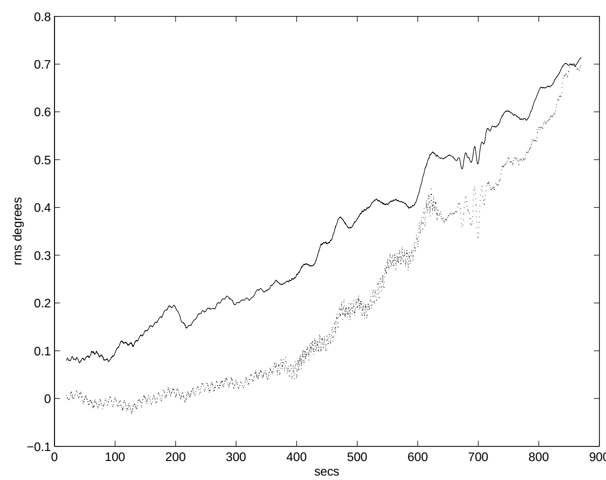

Fig. 8. Root sum square error with bias computed from observer (- - - -), and zero bias (——). Data has been smoothed using a 10 second averaging window.

VIII. Concluding Remarks

Since true values of the bias errors are unknown, the only possible test is to compare integrated body angular rates with know Euler angles. In our tests, the least squares technique was superior in minimizing Euler angle error (compare Figures 5 and 8). Yet we believe that overall, our experiments remain somewhat inconclusive. Although bias error is a major contributor to Euler angle error, other error sources are likely evident. These include scale factor and alignment errors. Further test will be conducted in which bias, scale factor, and alignment errors are estimated simultaneously.

Acknowledgments

The authors are grateful to Dr. Louis L. Whitcomb and Mr. David J. Smallwood of Johns Hopkins University for hosting our guidance system on the JHUROV, and for their assistance in obtaining the experimental data that appears in this paper. The authors also gratefully acknowledge the support of the Office of Naval Research through grant number N0001400WR20277.

References

[1] K. R. Britting, *Inertial navigation system analysis*, John Wiley and Sons, Inc., New York, 1971.

[2] T. I. Fossen, *Guidance and Control of Ocean Vehicles*, John Wiley and Sons, Ltd., England, 1994.

[3] M. S. Grewal, A. P. Andrews, *Kalman filtering: theory and practice*, Prentice Hall, New Jersey, 1993.

[4] A. J. Healey, E. P. An, D. B. Marco, "On Line Compensation of Heading Sensor Bias for Low Cost AUV Navigation", *Proceedings of IEEE AUV'98*, Cambridge, MA, August, 1998.

[5] E. Nebot, H. Durrant-Whyte, "Initial calibration and alignment of low-cost inertial navigation units for land vehicle applications," *Journal of Robotic Systems*, 16(2), pp. 81-92, 1999.

[6] S. Salcudean, "A globally convergent angular velocity observer for rigid body motion," *IEEE Transactions on Automatic Control*, Vol. 36, No. 12, 1991, pp. 1493-1497.

[7] S. Sukkarich, E. M. Nebot, H. F. Durrant-Whyte, "A high integrity IMU/GPS navigation loop for autonomous land vehicle applications," *IEEE Transactions on Robotics and Automation*, 15(3), pp. 572-578, 1999.

[8] D. H. Titterton, J. L. Weston, *Strapdown inertial navigation technology*, Peter Peregrinus Ltd. on behalf of the Institution of Electrical Engineers, United Kingdom, 1997.

[9] B. Vik, T. I. Fossen, "A Nonlinear Observer for Integration of GPS and Inertial Navigation Systems," *Modeling, Identification and Control*, Vol. 21, No. 4, pp. 193-208.

[10] C. E. Wick, D. J. Stilwell, "Design and testing of a miniature autonomous underwater vehicle," *Proceedings IEEE/MTS Oceans 2001*, Hawaii, 2001.

[11] X. Yun, E. R. Bachmann, R. B. McGhee, R. H. Whalen, R. L. Roberts, R. G. Knapp, A. J. Healey, M. J. Zyda, "Testing and evaluation of an integrated GPS/INS System for small AUV navigation," *IEEE Journal of Oceanic Engineering*, Vol. 24, No. 3, 1999, pp. 396-404.

Appendix

The USNA guidance package, including Litton IMU is briefly described. The guidance package was designed and constructed by a team of Midshipmen at the Unites States Naval Academy, including the second author. The interior electronics shelf of the guidance package is shown in Figure 9 and the water tight pressure vessel is shown in Figure 10. The pressure vessel contains an LN200 inertial measurement unit from Litton Guidance, a TCM2-50 electronic compass module from PNI, Inc., and a PC104 stack with CPU and A/D converters. The PC104 stack also contains an RS485 synchronous serial card from SeaLevel Inc. to enable frame-based IBM Synchronous Data Link Control protocol communications between the IMU and CPU. Externally, the guidance package communicates via a standard RS232 serial port and requires 24 volt DC power. The IMU generates acceleration and angular rate for each of three orthogonal axes at 400Hz. The PC104 stack computes the mean of 40 samples, which is transmitted through the RS232 port at 10 Hz.

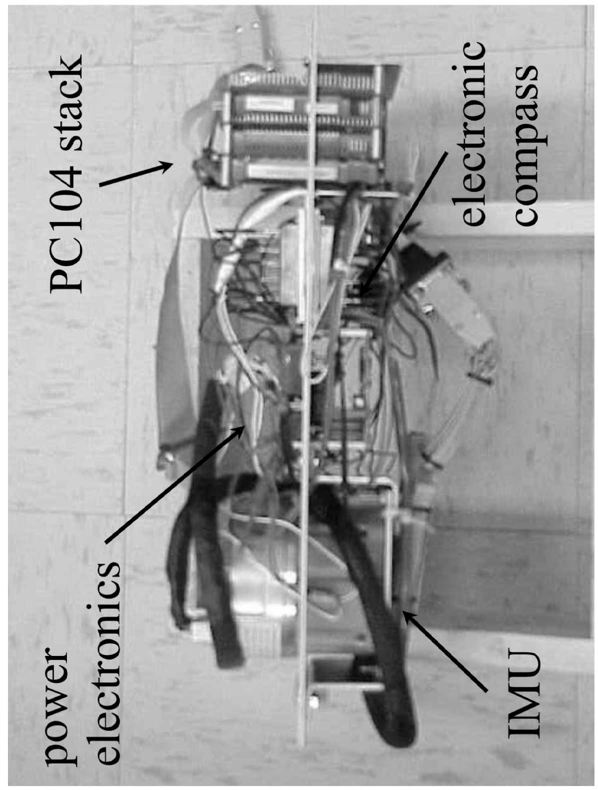

Fig. 9. Electronics shelf of the USNA inertial guidance package.

Fig. 10. USNA inertial guidance package mounted on the JHUROV.